Surface & Coatings Technology 358 (2019) 340–346

Contents lists available at ScienceDirect

Surface & Coatings Technology

journal homepage: www.elsevier.com/locate/surfcoat

Application of biofuel impurities and effect on the hot corrosion of yttria-stabilized zirconia thermal barrier coatings

Jorge H. Ramirez Velasco[a,*], Gozdem Kilaz[b], Hilkka I. Kenttämaa[c], Rodney W. Trice[a,*]

[a] School of Materials Engineering, Purdue University, West Lafayette, IN, United States
[b] School of Engineering Technology, Purdue University, West Lafayette, IN, United States
[c] Department of Chemistry, Purdue University, West Lafayette, IN, United States

ARTICLE INFO

Keywords:
YSZ
TBC
CMAS
Biofuel
Corrosion

ABSTRACT

The contaminants found in biofuels include alkali and alkaline metals along with sulfur, phosphorus and silicon oxides. Furthermore, while calcium-magnesium-aluminum silicates (CMAS) are typically ingested as particulate in middle-east theaters, the impurity list in biofuels includes the necessary elements to form CMAS without exposure to any environment. This is significant as CMAS is particularly destructive for operating temperatures above its melting temperature (~1250 °C), particularly affecting the lifetime of 7 wt%Y_2O_3-ZrO_2 (YSZ) thermal barrier coatings (TBCs). In the work reported currently, solutions containing the individual and unreacted constituents of CMAS were prepared and sprayed onto either air plasma sprayed (APS) or electron beam physically deposited (EB-PVD) TBCs and subsequently subjected to dynamic heating up to 1400 °C, simulating the deposit and thermal conditions of the biofuel impurities during combustion. Microstructure analysis revealed that the individual constituents of CMAS accelerated degradation of the TBCs compared to the same samples heated without impurities.

1. Introduction

Gas turbines are an essential element of the modern world, being used to generate electrical power or thrust in commercial and military aircraft. In an effort to improve gas turbine efficiency they have been operated at progressively higher temperatures, with ceramic thermal barrier coatings (TBCs) being employed in the combustion chamber to protect the underlying superalloy structure from temperature extremes. The processes used for depositing YSZ TBCs are typically either air plasma spray (APS) or electron beam physical vapor deposition (EB-PVD). APS coatings are typically used for large stationary components such as the combustion chamber walls while EB-PVD coatings are applied to small or rotating components such as blades and vanes. The most utilized TBC material is 7 wt% Y_2O_3-ZrO_2 (YSZ) due to its low thermal conductivity and the relatively slow destabilization kinetics of the as-deposited t'-ZrO_2 phase to c-ZrO_2 and t-ZrO_2 phase (and ultimately m-ZrO_2) upon heating [1]. With the maximum operating temperature of gas turbines increasing to 1250 °C and above, a new problem has emerged for TBCs that has been well documented over the last decade [2–4]. Calcium-magnesium-aluminum silicates or CMAS, a particulate common to the middle east regions or found in volcanic ash, can be pulled into a gas turbine. Depending on the composition of the particulate, it can melt and infiltrate into the TBC via the porous pathways in either the APS or EB-PVD microstructures. Upon cooling, the compliance difference between infiltrated and non-infiltrated coating regions causes residual stresses that can delaminate the infiltrated coating. Repeated heating/infiltration/cooling cycles can remove the entire TBC.

There is currently momentum to shift to the use of biofuels in gas turbines. For example, United Airlines flights between Los Angeles and San Francisco, have been using a blend of 70% Jet-A and 30% biofuel since 2016. Biofuels can be formed via numerous biomass processing approaches, using a multitude of different biomasses to include wheat, willow, and even olive waste [5]. It has been well established that contaminates found in fossil fuels such as Jet A can be incorporated into TBCs, ultimately hastening their failure through a variety of different corroding mechanisms. Contaminants found in fossil fuels include S, V, Na, Ca, K, P etc. [6]. With the use of biofuels, however, a new group of contaminants must be considered. It has been determined that the amount of impurities present in biofuels depend directly on the biomass source. The composition of impurities in the biomass source is highly variable due to its dependence on factors such as harvest season, composition of the soil, and drying temperature [7]. This list includes Al, Ba, Ca, Fe, K, Mg, Na, P and Si [8]. Inspection of this list reveals that

* Corresponding authors.
E-mail addresses: ramir134@purdue.edu (J.H. Ramirez Velasco), rtrice@purdue.edu (R.W. Trice).

https://doi.org/10.1016/j.surfcoat.2018.10.019
Received 28 April 2018; Received in revised form 16 September 2018; Accepted 7 October 2018
Available online 10 October 2018

those same elements found in particulate forms of CMAS are found as individual constituents in biofuels. Thus, a gas turbine operating with biofuels maybe exposed to the constituents of CMAS without ever being operated in a middle east or volcanic ash environment. While extensive studies of the effect of fossil fuel impurities have been performed previously [9], the effect of impurities and oxides of alkali and alkaline metals found in commercial and military biofuel blends (e.g. HEFA, FT-S8, SIP) is still unknown. Because of the growing importance of biofuels worldwide, a specific understanding of the possible negative effects of these impurities is extremely important to avoid premature failure of TBCs used in gas turbines.

In the work reported here, we have developed a methodology to incorporate the individual impurities found in biofuels into TBCs made either via APS or EB-PVD. The approach uses impurity "cocktails", solutions combining the impurities of interest that are subsequently sprayed on TBCs. Their effect on the microstructure is subsequently evaluated after heating/cooling in an ablation rig to temperatures of 1400 °C. The goal is to validate a methodology robust enough as to easily incorporate impurities that may arise from aviation fuels or external sources to ultimately understand the mechanisms of degradation when impurities are incorporated into a TBC. For such purposes in the presented case of study, a conventional 4-component CMAS composition was selected.

2. Experimental methods

2.1. Formulation and application of the impurity cocktails

According to Drexler et al. [10] different methodologies are used for testing the degradation of TBCs under high temperature and corrosive deposit conditions. When testing in a furnace, impurities of interest are commonly deposited over the sample surface in the form of a slurry. This approach for applying impurities is not suitable for burner rig testing, since the deposited paste will flake off without infiltrating the sample. Instead, a more effective approach for burner rigs consist of spraying an impurity powder directly in to the flame during the dynamic heating cycle. The challenges of this approach include monitoring the concentration of the deposited impurity species during the test and delineating between the thermo-chemical and thermo-mechanical effects on the sample microstructure. In this study, a low viscosity "impurity cocktail" was prepared which contained a known concentration of impurities. This cocktail was subsequently sprayed on the sample surface at a concentration of 1 mg/cm^2 prior to ablation testing. However, as the coatings investigated presently were porous, the impurity cocktail infiltrates the microstructure to an unknown depth that was not characterized prior to ablation testing.

Nitrates of the alkaline metals, including $Ca(NO_3)_2$ (Sigma Aldrich), $Mg(NO_3)_2$ (Sigma Aldrich), and $Al(NO_3)_3$ (Sigma Aldrich) are soluble in ethanol. Using these nitrates, and the pre-ceramic polymer $Si(OC_2H_5)_4$ (Sigma Aldrich), an impurity cocktail with a composition in mole percent of 33CaO-9MgO-6.5Al_2O_3-45SiO_2 was formulated with the assumption that each nitrate or silicate solution would oxidize upon heating according to:

$$2Ca(NO_3)_2 \rightarrow 2CaO + 4NO_2 + O_2$$

$$2Mg(NO_3)_2 \rightarrow 2MgO + 4NO_2 + O_2$$

$$4Al(NO_3)_3 \rightarrow 2Al_2O_3 + 12NO_2 + 3O_2$$

$$Si(OC_2H_5)_4 \rightarrow SiO_2 + 2C_2H_3OH + 2C_2H_4$$

This composition of CMAS chosen was based on the average of deposits on aircraft turboshafts shrouds as reported by Borom et al. [11] The conversion temperature of the reactions to produce the individual constituents of CMAS are all lower than 670 °C. The individual constituents of CMAS were dissolved in ethanol to make a 10% concentration of the impurities in solution. In the as-mixed cocktail there was no visual evidence of the formation of precipitates to suggest that the constituents reacted with one another or stratification of the added constituents suggesting they unmixed.

Prior to deposition of the impurity cocktail, the coatings were heated up to 100 °C by placing a hot plate in direct contact with the coating substrates. An air brush kit, with the air pressure held constant at 0.2 MPa, was used to spray the impurity cocktail. Impurity cocktails were sprayed on heated TBC/substrates in intervals of 5 s followed by 3 s of no spray to facilitate ethanol solvent vaporization. The concentration of the impurity (not including the ethanol carrier) was constant at 1 mg/cm^2. Samples were dried at room temperature for 24 h and their weight monitored to verify that the ethanol had completely evaporated prior to the ablation cycle. The impurities were re-applied after each ablation cycle to a concentration of 1 mg/cm^2. The expected decomposed oxide products (CMAS) infiltrating the coatings in every spraying/ablation cycle was of a concentration of 0.26 mg/cm^2.

Table 1
As-received specifications of APS and EB-PVD TBCs.

Specification	APS	EB-PVD
Geometry	Button Ø 25.4 mm	Button Ø 25.4 mm
Top coat material	7YSZ	7YSZ
Top coat thickness	760 μm	130 μm
Bond coat material	CoNiCrAlY	PtAl
Bond coat thickness	230 μm	50 μm
Substrate alloy	Inconel 718	Rene N5
Total thickness	4 mm	3.5 mm

2.2. TBC coatings evaluated

Table 1 presents the APS and EB-PVD TBC coating systems (topcoat of 7 wt% Y_2O_3-ZrO_2, and a bondcoat of either CoNiCrAlY or PtAl) evaluated in the current study. Each TBC system was applied to 25 mm diameter superalloy substrate. The APS TBC coating was produced by Praxair Surface Technologies. The topcoat of YSZ was processed to have a dense vertically-cracked (DVC) microstructure. The vertical cracks in the APS TBC are designed to simulate the columns observed in EB-PVD coatings. A CoNiCrAlY bondcoat was used for the APS TBCs, sprayed first on the Inconel 718. The EB-PVD TBC was supplied by GE, with a topcoat of YSZ, a bondcoat of PtAl, and a superalloy of Rene N5. Cross-sectional and surface views of each coating are shown in Fig. 1. The cross-sectional image of the APS TBC (Fig. 1a) show vertical cracks, while the cross-sectional image of the EB-PVD coatings shows the expected columnar microstructure.

2.3. Ablation and characterization

In the current study, the deposition of the impurities on the TBCs was performed prior to ablation cycling, affording better control of the impurity composition, surface impurity concentration and a partial separation of the mechanical effect degradation (e.g. erosion) from the thermochemical degradation effect. To ablate the samples a 5-W Victor welding nozzle was used for the torch with an acetylene to oxygen ratio of 10:12 l per minute. Samples were positioned in the ablation rig using graphite plates that touched the top and bottom of the sample. This set-up allowed the complete front face of each sample to be exposed to the flame. The backside of the samples was free of obstructions to permit natural convection cooling of the substrate.

The temperature of the front face (i.e. the TBC surface temperature), was measured in intervals of 1 s using an infrared pyrometer (Omega OS3753) with a near-infrared (NIR) wavelength of 1.55 μm. As noted by Manara et al. [12] the low emissivity and high reflectivity of YSZ influence the infrared-optical characteristics of TBCs, affecting the precision of measurements taken by a pyrometer. Particularly, it has been observed that the infra-red energy measured comes mostly from below

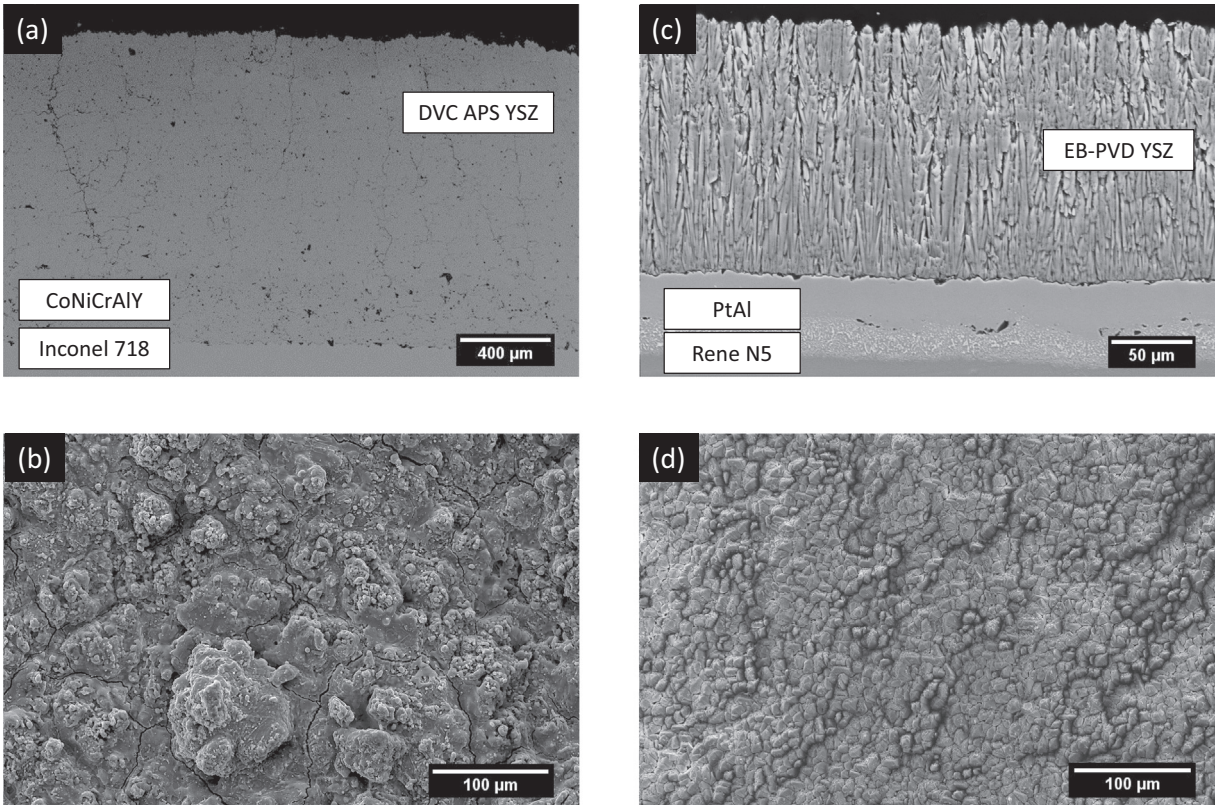

Fig. 1. SEM micrographs showing APS and EB-PVD TBCs in the as received condition. Images (a) and (b) show the cross-section and top surface of the APS coatings studied. Images (c) and (d) show the cross-section and top surface of the EB-PVD coatings studied.

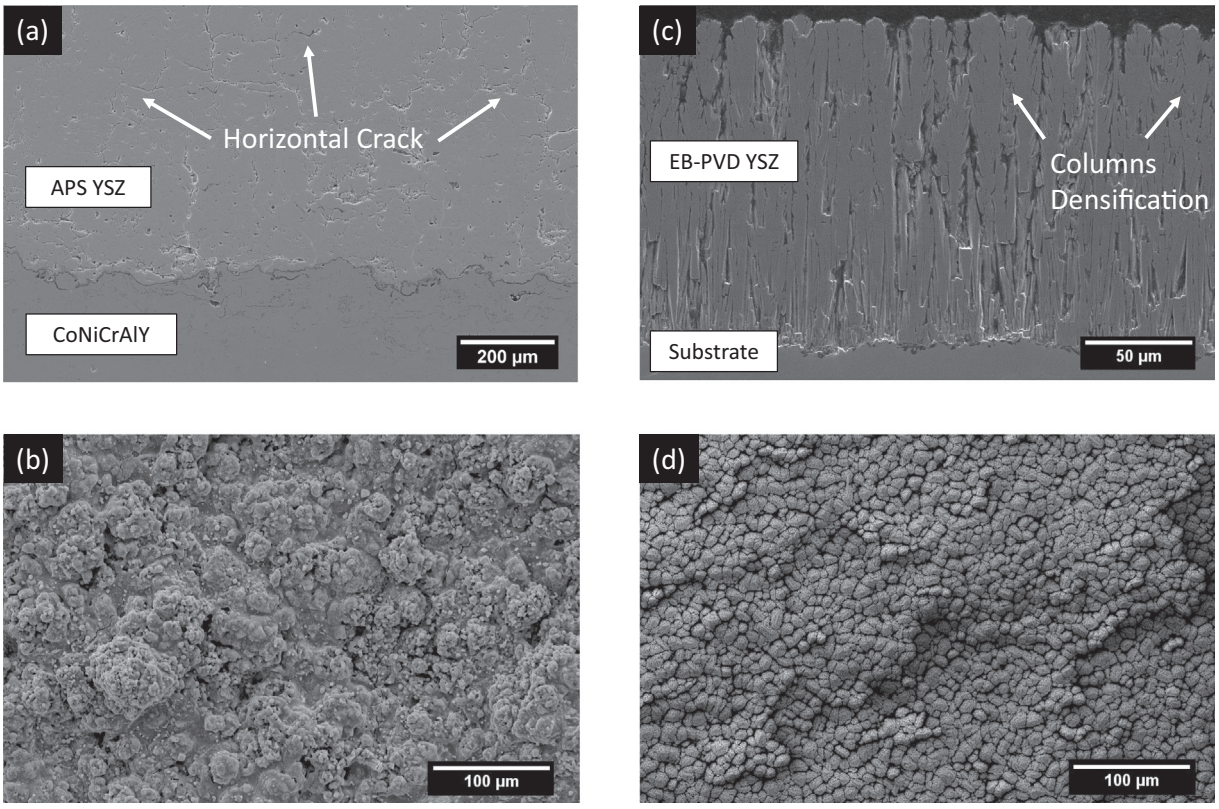

Fig. 2. APS TBC (a) cross section and (b) surface after ablation for 30 min without impurities at 1400 °C and EB-PVD TBC (c) cross section (d) and surface after ablation without impurities for 20 min at 1250 °C.

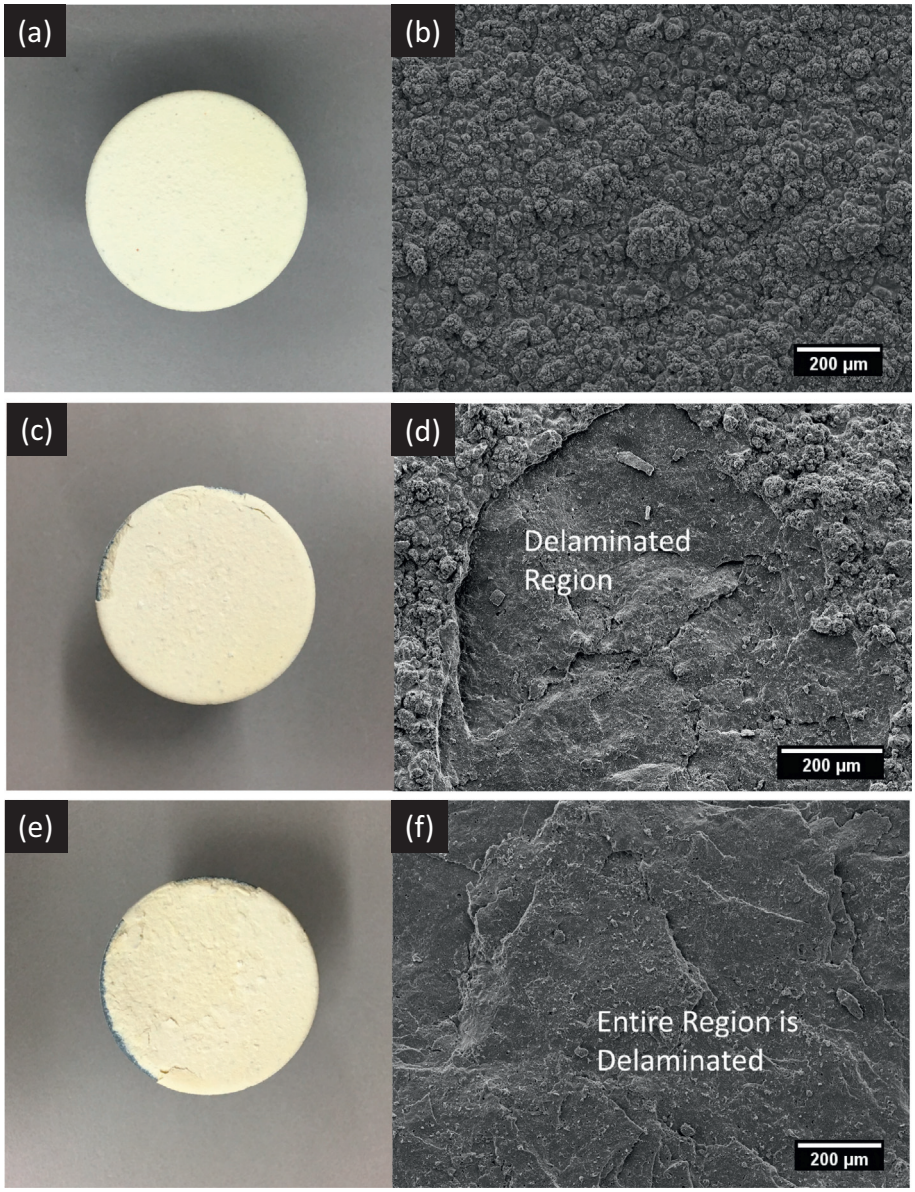

Fig. 3. APS sample with CMAS impurities, ablated for 10 min (a,b), 20 min (c,d) and 30 min (e,f) at 1400 °C.

the surface of the coating and not from the surface directly exposed to the flame. Thus, the actual surface temperature is likely higher than that measured and reported in the current data set.

The back-surface temperature was measured using a sheathed Type K thermocouple, with a single point in contact with the superalloy substrate. The thermocouple was positioned behind the region where the flame was positioned. Front face temperatures were maintained between 1400 °C to 1500 °C for APS and 1250 °C to 1300 °C for EB-PVD coatings. X-ray diffraction investigations in the 2θ range of 72 to 76° revealed that EB-PVD coatings without added impurities were rapidly transforming the as-deposited t'-ZrO_2 to other zirconia phases at 1400 °C. Thus, a lower ablation temperature of 1250 °C–1300 °C was chosen. The APS coatings without added impurities remained t'-ZrO_2 after the 30-min ablation at 1400 °C; thus, an ablation temperature of 1400 °C was used for the APS coatings. The back temperature of the substrates never exceeded 1000 °C for either TBC, avoiding substrate phase changes and melting temperatures reported for Inconel 718 and Rene N5 [13,14]. After each cycle samples were allowed to cool down to room temperature by air convection. APS and EB-PVD samples were ablated in 10-min cycles for a total ablation time of 30 and 20 min, respectively. The impurity was reapplied in a 1 mg/cm^2 concentration after each ablation cycle.

As received and after ablation X-Ray Diffraction (XRD) patterns were collected with a *Bruker D8 Focus* diffractometer. Samples were analyzed with an X-Ray copper source (λ = 0.1544 nm), a 2θ interval between 20° to 90° and a scan speed of 3° per minute in increments of 0.01° per step. Additionally, SEM micrographs of as-received coatings and after ablation were taken. Cross-sectional images of each coating were prepared by mounting the sample in epoxy and polishing down through 5 µm using a diamond paste. For both cross sectional and surface SEM analysis, a carbon coating was applied to the samples to avoid sample charging.

3. Results and discussion

3.1. Effect of thermal cycling on APS and EB-PVD coatings (no impurities added)

Fig. 2 shows APS and EB-PVD TBC samples and a topological micrograph for each after being ablated for 30 min and 20 min,

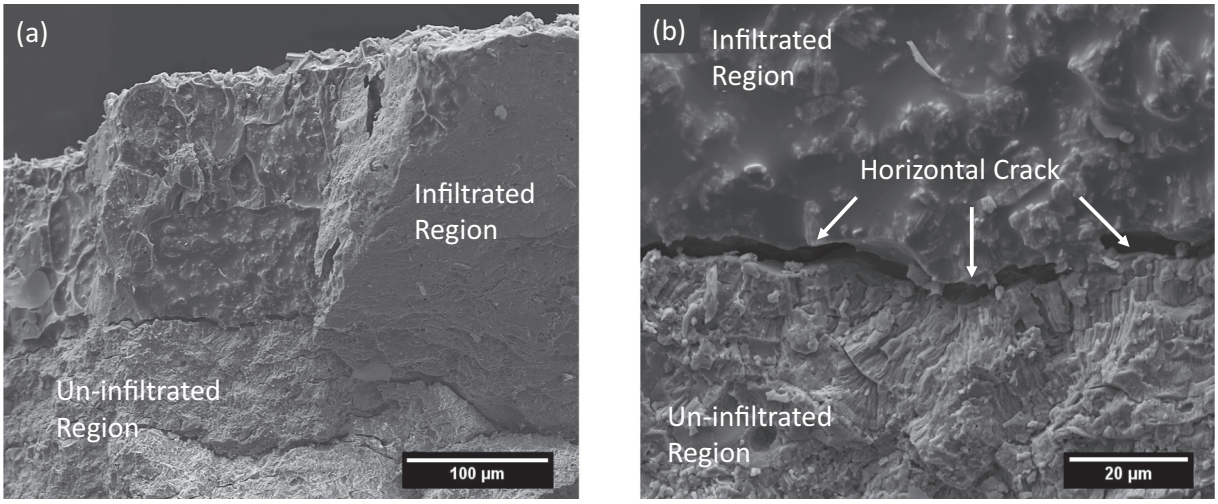

Fig. 4. SEM micrographs of a piece of delaminated APS coating following 30 min of ablation. There are regions that have clearly been completely infiltrated by the reaction products. Horizontal cracks separate infiltrated from un-infiltrated regions in the coating.

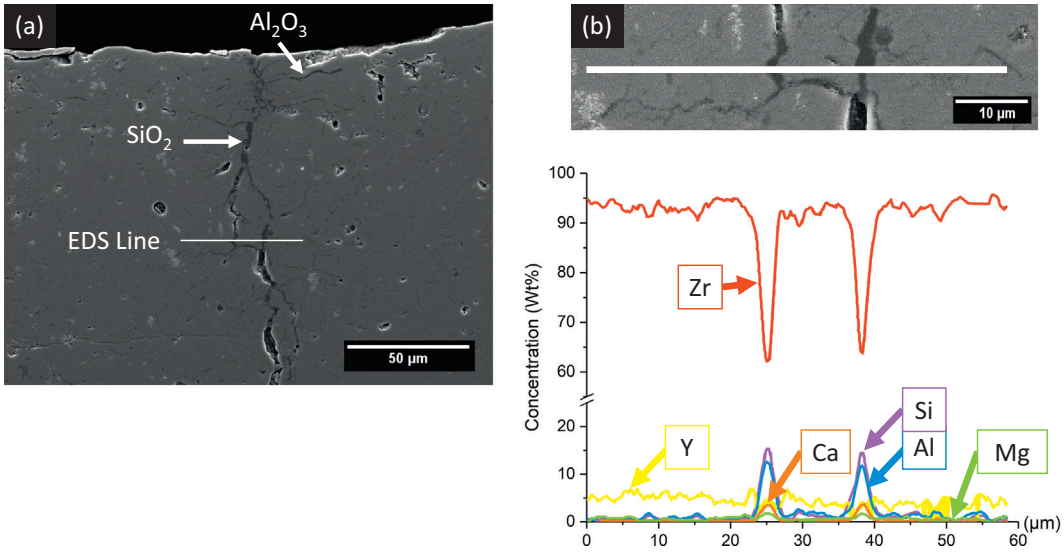

Fig. 5. a) SEM micrograph of an APS YSZ top coating after 30 min of ablation testing showing the infiltration of a glassy reaction product. b) Shows an enlarged area of this coating, with the corresponding EDS scan and the resulting elemental analysis.

respectively. These samples did not have any impurity applied and, thus, they represent the baseline condition for each TBC type. Neither the APS or EB-PVD TBC samples showed significant degradation after being ablated. Cross sections of each coating after ablation, revealed the formation of small horizontal cracks in the APS sample due to thermal cycling (Fig. 2a), and microstructural densification in the EB-PVD TBC (Fig. 2c). Comparison of Fig. 1b with Fig. 2b reveals no difference in the APS coating surface before and after ablation. Similar observations were made for the EB-PVD coatings, as is seen in Fig. 1d and Fig. 2d.

3.2. Combined effect of thermal cycling and CMAS impurities on APS and EB-PVD coatings

3.2.1. APS TBCs

Fig. 3 shows the changes in the APS TBC samples after each 10-min cycle, with CMAS impurities added prior to each successive cycle. Fig. 3b, d, and f show the top surface of the coating. After the first thermal cycle of 10 min to 1400 °C, Fig. 3a and b show no difference in comparison to the sample surface ablated with no impurities after 30 min at 1400 °C (Fig. 2a and b). After reapplication of the impurity cocktail and another 10 min of ablation, evidence of spallation and crack formation was apparent (Fig. 3c and d). Fig. 3d shows a region on the surface where part of the coating has delaminated. Finally, after reapplication of the impurity solution and a total of 30 min of ablation, large-scale spallation was clearly visible in the sample (Fig. 3e and f). In contrast, the sample that was ablated with no impurities never exhibited coating spallation even after 30 min of ablation (Fig. 2b).

The mechanism by which the APS TBC delaminates can be explained by analyzing the spallation debris. Fig. 4a shows a piece of debris in cross-section. There is clearly a glassy phase that has infiltrated the coating, with a clear demarcation observed between the infiltrated and un-infiltrated parts of the coating. More detailed observations of debris as in Fig. 4b show horizontal cracks right next to areas where the infiltrated impurities solidified, leading to the conclusion that the layer by layer delamination of the TBC is cause by partial infiltration, solidification and horizontal crack formation in the TBC during every heating cycle.

Fig. 5a shows a polished cross-section of the APS TBC after 30 min of ablation time showing filled vertical cracks. Note that this sample had the impurity cocktail applied 3 times. The vertical crack in this

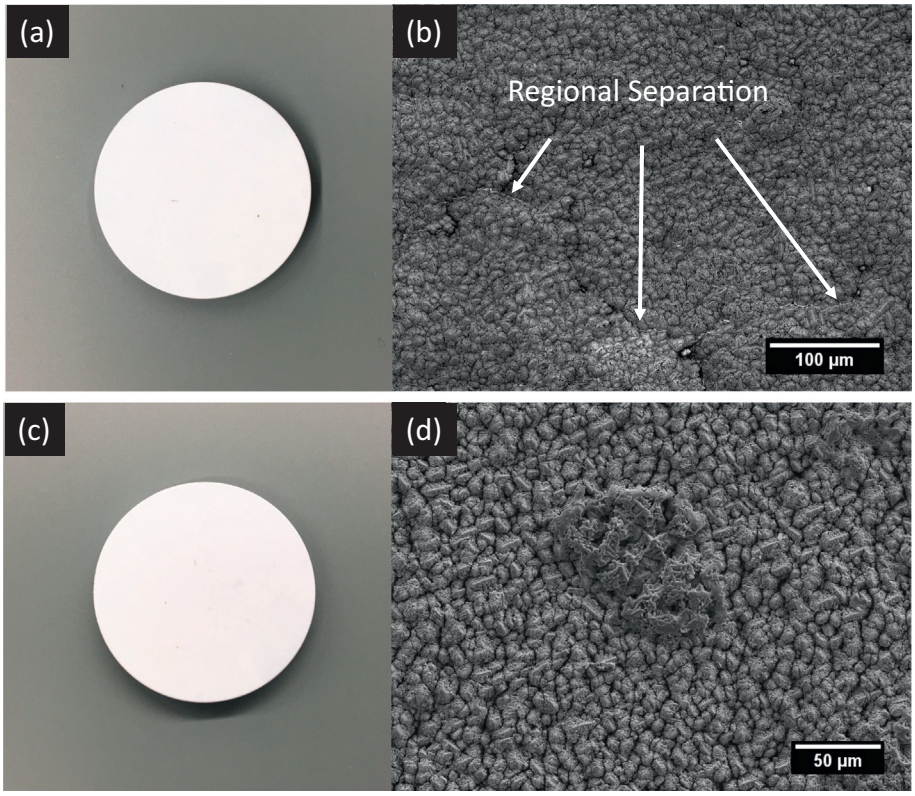

Fig. 6. EB-PVD sample with CMAS impurities ablated for 10 min (a, b) and 20 min (c, d).

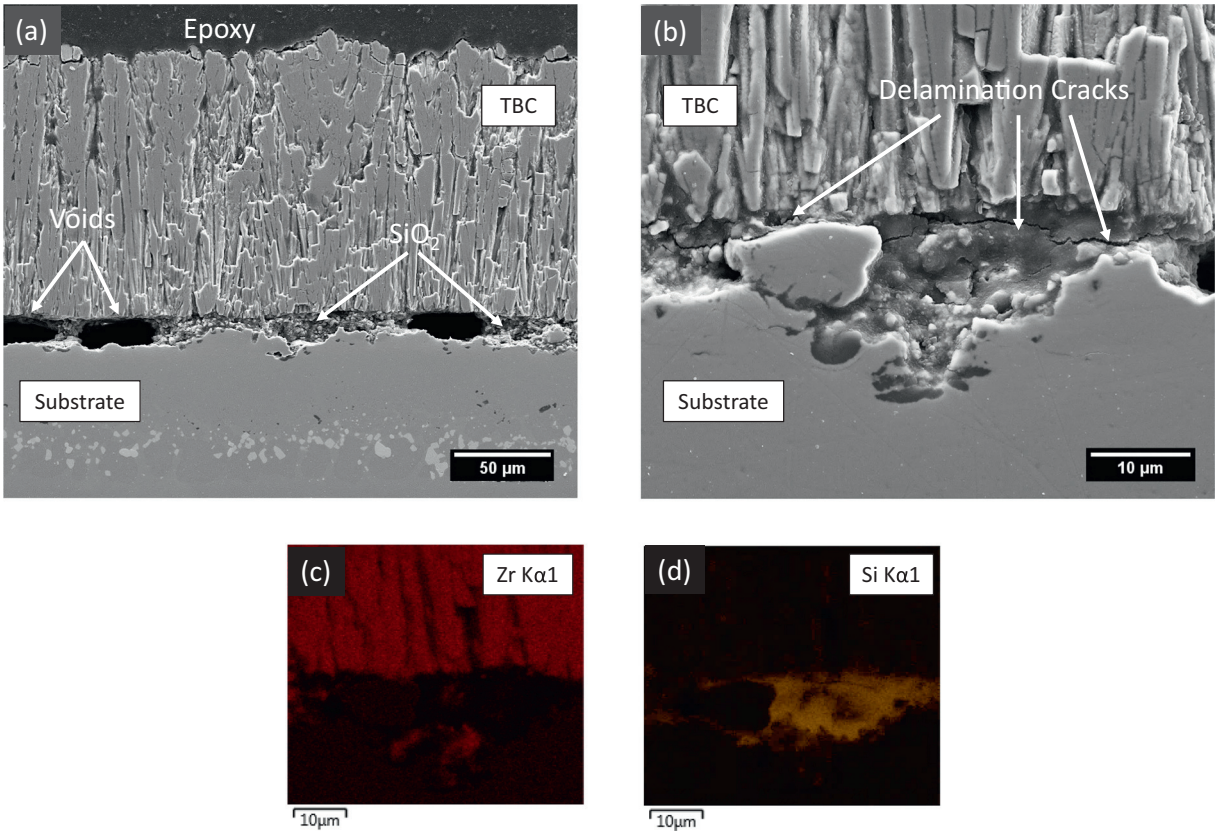

Fig. 7. EB-PVD TBC with impurity cocktail and 20 min of ablation. Cross section (a) and close view of the infiltrated products (b) with the corresponding element maps (c and d) for Zr(Lα1) and Si(Kα1).

micrograph has clearly been filled with a secondary phase. Also indicated in Fig. 5a is a region analyzed using a qualitative energy dispersive spectroscopy (EDS) line scan. Fig. 5b shows a close-up of this region. The qualitative EDS revealed the presence of the added impurities within the vertical cracks of the TBC. The strong Si signal suggests the presence of a silica-containing material. Similarly, peaks associated with the presence of Al, Ca and Mg were also noted in the vertical cracked regions suggesting that the Si, Al, Ca, and Mg have reacted together. Furthermore, zirconium was still observed in the vertically cracked regions, indicating that it was somewhat dissolved by the presence of the glassy product [15,16,17].

3.2.2. EB-PVD TBCs

Fig. 6a–d shows the combined effects of thermal cycling and the addition of the impurity solution on EB-PVD TBCs. After the application of impurities and 10-min ablation near 1300 °C, SEM micrographs revealed column separation in different regions (Fig. 6b) as compared to the EB-PVD sample heated to 1300 °C with no impurities (Fig. 2d). Reapplication of the impurity followed by another 10-min ablation cycle caused no apparent delamination of the coating (Fig. 6c), in the surface, limited areas with reaction products were observed (Fig. 6d).

Fig. 7a shows the polished cross-section of the EB-PVD TBC after 20 min of ablation and two applications of the impurity cocktail, along with a detailed view of the reaction products near the EB-PVD coating/bondcoat interface (Fig. 7b). Fig. 7c show elemental map for Si at the interface shown in Fig. 7b. Fig. 7a reveals regions of severe attack in the TBC/substrate interface, as well as void regions. Comparison of Fig. 7a to a coating ablated 20 min with no impurities (Fig. 2c) reveals stark differences in the interface microstructure. Moreover, Fig. 7b, which was taken near the coating/bondcoat interface, along with the corresponding EDS map for Si, shows that significant concentrations of silica-containing phases are in this region. The location of the impurities strongly indicates full infiltration of the impurities through its entire thickness, reaching the denser bondcoat. As a reminder, the APS samples did not experience penetration of the modified silica phase through its thickness. This is in part due to the thicker APS top coat, which suggest that a larger amount of impurities is necessary to saturate the APS TBC microstructure (e.g. the open porosity) and totally infiltrate the coating. Furthermore, close inspection of Fig. 7b shows a horizontal crack developing in this silica-rich region, a precursor to delamination of the coating.

The location of the impurities products is consistent with the Zhao et al. [18] correlation of liquid permeability/intercolumnar pore fraction for the infiltration of particulate forms of CMAS in TBCs, with correlations made using similar thicknesses and sample compositions to those employed for this study. In their studies the columnar microstructure of the EB-PVD TBC favored the infiltration of the impurities, achieving full infiltration of the impurities (i.e. reaching the substrate) seconds after melting of the particulate form of CMAS. Thermochemical studies of molten CMAS with YSZ TBCs performed by Krämer et al. [19] observed that the full infiltration of molten CMAS in EB-PVD prepared coatings is accompanied by horizontal cracks at the topcoat/bondcoat interface, similar to the observations in Fig. 7b. Nevertheless, it is important to note that the infiltration of the impurity was not accompanied by a degradation of the columnar tips as suggested by previous literature. As noted by Vidal-Sétif et al. [20] tip degradation phenomena are present when a large volume of CMAS is present, opposite to the methodology proposed in this study where the amount of impurities is limited during each cycle.

4. Conclusions

A methodology to incorporate impurities found in aviation fuels and external contaminants has been developed by mixing alkali and alkaline nitrates and a silicon-containing preceramic polymer in an ethanol solution to form impurity cocktails. For this study, the impurity cocktail was designed to match the composition of the individual constituents found in particulate forms of CMAS. The solution was sprayed on both APS and EB-PVD TBCs, and its effect on the microstructure was evaluated after successive ablation cycles. The APS TBC exhibited extreme delamination, with the vertical cracks being filled by the modified silica glass, the oxidation product of the impurity cocktail. Each ablation cycle caused increased delamination. The oxidation product associated with impurity cocktail interacted with the EB-PVD TBC differently than in the APS TBC, presumably due to differences in the thickness of the two different TBCs layers and the tortuosity of the pores. However, micrographs revealed nucleation and propagation of horizontal cracks in the oxide products for both coating types, features commonly observed as precursors for delamination.

Acknowledgments

This work was supported as part of Purdue's NEPTUNE Center for Power and Energy, funded by the Office of Naval Research under Award Number N000141613109. Furthermore, the authors would like to thank GE (Dr. Doug Konitzer) for providing the EB-PVD TBCs and Praxair Surface Technologies (Dr. Chris Petorak) for providing the APS TBCs.

References

[1] R.A. Miller, Thermal barrier coatings for aircraft engines: history and directions, J. Therm. Spray Technol. 6 (1) (1995) 35–42.
[2] S. Krämer, S. Faulhaber, M. Chambers, D.R. Clarke, C.G. Levi, J.W. Hutchinson, A.G. Evans, Mechanisms of cracking and delamination within thick thermal barrier systems in aero-engines subject to calcium-magnesium-alumino-silicate (CMAS) penetration, Mater. Sci. Eng. A 490 (1–2) (2008) 26–35.
[3] N.P. Bansal, S.R. Choi, Properties of CMAS glass from desert sand, Ceram. Int. 41 (3) (2015) 3901–3909.
[4] M.H. Vidal-Setif, N. Chellah, C. Rio, C. Sanchez, O. Lavigne, Calcium-magnesium-alumino-silicate (CMAS) degradation of EB-PVD thermal barrier coatings: characterization of CMAS damage on ex-service high pressure blade TBCs, Surf. Coat. Technol. 208 (2012) 39–45.
[5] S.V. Vassilev, D. Baxter, L.K. Andersen, C.G. Vassileva, An overview of the chemical composition of biomass, Fuel 89 (5) (2010) 913–933.
[6] Tom I.-P. Shih, Vigor Yang, Turbine Aerodynamics, Heat Transfer, Materials, and Mechanics, (2014) (Print).
[7] W.R. Livingston, Fouling corrosion and erosion, in: A.V. Bridgwater, H. Hofbauer, S. van Loo (Eds.), Thermal Biomass Conversion, CPL Press, 2009, pp. 157–176.
[8] N.J. Simms, P.J. Kilgallon, J.E. Oakey, Degradation of heat exchanger materials under biomass co-firing conditions, Mater. High Temp. 24 (4) (2007) 333–342.
[9] P. Mohan, Environmental Degradation of Oxidation Resistant and Thermal Barrier Coatings for Fuel-Flexible Gas Turbine, M.S. University of Central Florida, 2010.
[10] J.M. Drexler, A. Aygun, D. Li, R. Vaßen, T. Steinke, N.P. Padture, Thermal-gradient testing of thermal barrier coatings under simultaneous attack by molten glassy deposits and its mitigation, Surf. Coat. Technol. 204 (16–17) (2010) 2683–2688.
[11] M.P. Borom, C.A. Johnson, L.A. Peluso, Role of environment deposits and operating surface temperature in spallation of air plasma sprayed thermal barrier coatings, Surf. Coat. Technol. 86–87 (1996) 116–126.
[12] J. Manara, M. Zipf, T. Stark, M. Arduini, H.P. Ebert, A. Tutschke, A. Hallam, J. Hanspal, et al., Long wavelength infrared radiation thermometry for non-contact temperature measurements in gas turbines, Infrared Phys. Technol. 80 (2017) 120–130.
[13] G.A. Knorovsky, M.J. Cieslak, T.J. Headley, A.D. Romig, W.F. Hammetter, INCONEL 718: a solidification diagram, Metall. Trans. A. 20 (10) (1989) 2149–2158.
[14] R.J.E. Glenny, J.E. Northwood, A.B. Smith, Materials for gas turbines, Int. Mater. Rev. 20 (1) (1975) 1–28.
[15] P. Mohan, T. Patterson, B. Yao, Y. Sohn, Degradation of thermal barrier coatings by fuel impurities and CMAS: Thermochemical interactions and mitigation approaches, J. Therm. Spray Technol. 19 (1–2) (2010) 156–167.
[16] F. Abe, S. Muneki, K. Yagi, Tetragonal to monoclinic transformation and microstructural evolution in ZrO2–9.7 mol% MgO during cyclic heating and cooling, J. Mater. Sci. 32 (2) (1997) 513–522.
[17] C.G. Levi, J.W. Hutchinson, M.-H. Vidal-Sétif, C.A. Johnson, Environmental degradation of thermal-barrier coatings by molten deposits, MRS Bull. 37 (10) (2012) 932–941.
[18] H. Zhao, C.G. Levi, H.N.G. Wadley, Molten silicate interactions with thermal barrier coatings, Surf. Coat. Technol. 251 (2014) 74–86.
[19] S. Krämer, J. Yang, C.G. Levi, C.A. Johnson, Thermochemical interaction of thermal barrier coatings with molten CaO–MgO–Al2O3–SiO2 (CMAS) deposits, 3175 (2006) 3167–3175.
[20] M.H. Vidal-Sétif, C. Rio, D. Boivin, O. Lavigne, Microstructural characterization of the interaction between 8YPSZ (EB-PVD) thermal barrier coatings and a synthetic CAS, Surf. Coat. Technol. 239 (May) (2014) 41–48.